

Reactions of Hydroxyl Radicals on Titania, Silica, Alumina, and Gold Surfaces

Myeong Suh, Paul S. Bagus, Sergei Pak, Michael P. Rosynek, and Jack H. Lunsford*

Department of Chemistry, Texas A&M University, College Station, Texas 77843

Received: October 13, 1999; In Final Form: January 20, 2000

Reaction probabilities of OH• radicals under steady state conditions were determined over TiO₂ (anatase and rutile), SiO₂ (fused quartz), α-Al₂O₃, and Au surfaces. The OH• radicals were produced from water in a microwave cavity and were detected by laser-induced fluorescence spectroscopy. At 308 K the reaction probabilities were 2×10^{-4} for TiO₂ (anatase and rutile), 2×10^{-3} for SiO₂, 5×10^{-3} for α-Al₂O₃, and $> 3 \times 10^{-2}$ for Au. The relative rate of H₂O₂(aq) decomposition was found to follow the sequence Au > α-Al₂O₃ > TiO₂ ≈ SiO₂, which, except for TiO₂, follows the sequence found for the OH• radical reaction probability. For all of the materials except TiO₂, a radical mechanism is proposed which describes a common set of reactions for the removal of OH• and the decomposition of H₂O₂. The first step in this mechanism is the coupling of OH• radicals to form H₂O₂. The overall rate of reaction for both OH• removal and H₂O₂ decomposition depends on the concentration of OH on the surface. A theoretical analysis using a cluster model for an Au surface has shown that the OH–Au chemisorption bond is dominantly ionic with the OH radical becoming an OH[−] anion. The adsorption energy may be as large as 155 kJ mol^{−1}. With TiO₂ as a catalyst and H₂O₂ as a reagent, an alternate mechanism that involves redox chemistry is believed to occur.

I. Introduction

It has long been known that radicals, formed in the gas phase, may react on the surface of a vessel, and thereby influence the kinetics of the system.¹ The effects of such “wall reactions” are usually minimized by coating the surface of the vessel with a relatively inert material. In certain cases, a surface may be both a source and a sink for gas phase radicals. For example, in the oxidative coupling of methane, methyl radicals that are formed on a catalytic surface enter the gas phase where they may couple to form ethane, or they may react back with the surface and subsequently be converted to carbon dioxide.² For selective coupling, it is desirable to minimize these secondary reactions with the surface.

Many of the same catalysts that are capable of forming methyl radicals also produce hydroxyl radicals from the reaction of H₂O with O₂ at elevated temperatures (e.g., 1100 K).³ These surface-generated gas-phase radicals may be important intermediates in catalytic combustion. As pointed out by Gershenson et al.,⁴ the reactions of OH• radicals with silica, alumina, and other metal oxide aerosols may play a role in atmospheric chemistry; however, atmospheric models often neglect these heterogeneous reactions. Fisher and co-workers^{5,6} have observed OH• radicals during plasma-enhanced chemical vapor deposition of SiO₂ from tetraethoxysilane and molecular oxygen, which is a process that is extensively used in the microelectronics industry. They suggest that the OH• radicals may influence the formation of the SiO₂ and the nature of the surface by creating silanol groups, which are undesirable for electronic applications. Finally, hydroxyl radicals are believed to be intermediates in the aqueous photooxidation of hydrocarbons over TiO₂ and other metal oxides. Surface reactions of OH• with the metal oxide would clearly be a significant factor in the photooxidation process.

Although the formation of OH• radicals at surfaces is now well established,^{3,7–10} little is known about their removal rate or the mechanism by which this occurs. Buss and co-workers¹¹ studied the reactions of OH• radicals, formed in a pure H₂O

plasma, with an oxidized Si₃N₄ material and poly(methyl methacrylate). The surface of the Si₃N₄ apparently was partially hydroxylated. The OH• reactivity, which is defined as the ratio of OH• radicals that react on the surface to the total flux of OH• incident on the surface, decreased from 0.57 ± 0.05 at 300 K to 0.00 ± 0.05 at 500 K, with an activation energy of -2.9 kcal mol^{−1}. A mechanism was proposed in which OH• radicals abstract hydrogen from silanol groups on the surface to form water. Curiously, the reactivity at the poly(methyl methacrylate) surface was the same at 300 K (0.6 ± 0.1) as that found on the oxidized Si₃N₄. Subsequently, Fisher and co-workers^{5,6} determined the reactivity of OH• radicals during plasma-enhanced chemical vapor deposition. Over SiO₂, they reported a reactivity of 0.41 ± 0.04 at 300 K. By contrast, using a different system, Gershenson et al.⁴ observed a reactivity at ca. 300 K of $(5.6 \pm 2) \times 10^{-3}$ over quartz that had been treated with hydrofluoric acid. Obviously, the two values for reactivity on SiO₂ are quite different.

In the work reported here, reaction probabilities, which are defined the same as the “reactivities” described above, were determined for OH• radicals interacting with silica (fused quartz), alumina (α), titania (anatase and rutile), and gold. The importance of OH• radical reactions with the oxides has been noted; gold was chosen as a representative metal that does not form a surface oxide, which is important since experiments were not carried out under UHV conditions. Insight into the mechanism for the surface reactions was provided by a parallel study on H₂O₂ decomposition over these materials.

II. Experimental Methods

The SiO₂ (QSI, 99.9%) used in this study was in the form of cylinders, 2 mm in diameter and 2 mm in length. The α-Al₂O₃ (Coors) similarly was in the form of cylinders. The cylinders, with an average length of 2 mm, were broken from a 1 mm diameter rod. The gold sample was prepared by coating the SiO₂ cylinders in a plasma discharge for 90 min at a discharge current

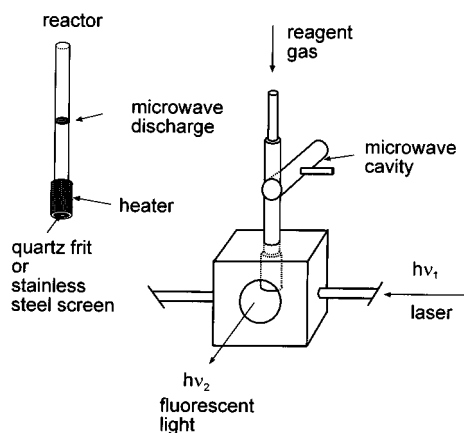


Figure 1. A schematic representation of the reaction cell showing the location of the sample and the microwave discharge.

of ca. 10 mA. Argon was used as a discharge gas. During deposition, the cylinders were turned to achieve uniform coverage. The resulting cylinders were a bright gold color, which indicates multilayer deposition. The silica-, alumina-, or gold-coated cylinders were loaded onto a stainless steel screen as described below. Typically, for silica and alumina the bed thickness was ~ 1.3 cm, but it was less than half this value for the gold-coated samples.

The anatase and rutile forms of TiO_2 (Alfa Aesar, 99.9% for anatase and 99+% for rutile) were obtained as loose powders having surface areas of 8.7 and 4.8 $\text{m}^2 \text{g}^{-1}$, respectively. The TiO_2 was added to a fused-quartz frit by means of a dilute aqueous slurry that contained 80 mg of TiO_2 in 40 mL of water. The slurry was poured through the frit, and a fraction of the TiO_2 was retained. After drying the frit and the TiO_2 , the amount of TiO_2 was determined by weight change. If more TiO_2 was desired, the process was repeated.

Hydroxyl radicals were formed by passing a gas stream containing H_2O and He through a microwave cavity. Helium at a flow rate of 0.55 mL s^{-1} (STP) was saturated with water vapor at 298 K. The partial pressure of the water was reduced from 24 to ~ 0.3 Torr by means of a valve and a vacuum pump. The gas mixture flowed through a 10 mm i.d. fused-quartz tube that had been coated with a 40% phosphoric acid solution and dried in air. This procedure significantly decreased the loss of OH^\bullet radicals due to the reaction with the wall. At the outlet of the tube was either a coarse fused-quartz frit of 1.5 mm thickness, which contained the TiO_2 , or a stainless steel wire screen that had 60% open area. The region around the frit or the screen was electrically heated. The microwave cavity was located 12 cm above the exit of the fused-quartz reactor as depicted in Figure 1. A microwave generator (Ophos Instrument model MP64) was operated at a power level of 10 W.

The concentration of hydroxyl radicals was determined by laser-induced fluorescence (LIF) spectroscopy. The system was essentially the same as that described previously,³ except the fused-quartz cell was replaced by a stainless steel box that was 13 cm on a side. The fused-quartz tube entered the box through a fitting and was positioned such that the bottom of the frit or the wire screen was 1 cm above the laser beam. Optical windows were added to the cell so that the laser beam could pass through it and the fluorescence could be detected. The $\text{A}^2\Sigma^+(\nu=0) \leftarrow \text{X}^2\Pi(\nu=0)$ transition (~ 308 nm) of the hydroxyl radicals was excited by light from a frequency-doubled tunable dye laser that was pumped by the second harmonic of a Q-switched Nd:YAG laser (Quantel) operating at 2 Hz. The output laser has a line width of 0.3 cm^{-1} and a pulse width of 5 ns, with about

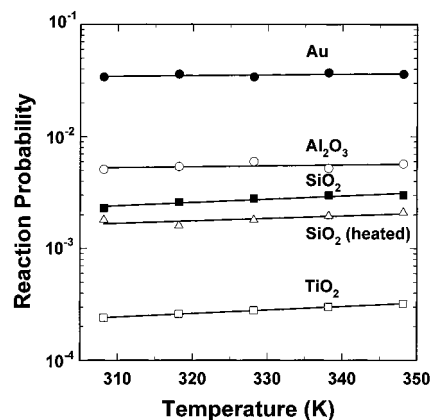


Figure 2. Reaction probability for OH^\bullet over TiO_2 (anatase), SiO_2 , $\alpha\text{-Al}_2\text{O}_3$, and Au as a function of temperature. SiO_2 (heated) refers to fused quartz that had been treated in air at 1173 K.

0.02 mJ/pulse. The fluorescence from the excited OH^\bullet radicals was collected at 90° from the laser beam and was detected by a photomultiplier tube (PMT). The signal output from the PMT was sent to a Q-switch-triggered digital oscilloscope (Tektronix model TDS520C). The $\text{Q}_1(4)$ rotational transition, which is relatively insensitive to temperature, was used as a measure of the hydroxyl radical concentration.

Hydrogen peroxide decomposition rates were obtained using a 30% aqueous solution of H_2O_2 (EM Science). Twenty-five milliliters of solution was placed in a 500 mL three-neck flask which was enclosed in aluminum foil to limit the amount of light that reached the catalyst. The temperature of the stirred solution was raised to 323 K, the catalyst was added, and the volume was isolated. The reaction rate was determined from the pressure increase, which was measured with a pressure gauge (Validyne). Except for the gold, the catalysts were the same as those described previously. Under the reaction conditions the gold film on the fused-quartz cylinders rubbed off; therefore, a section of gold foil (Johnson Matthey, 99.95%) was used as the catalyst.

III. Results

Reaction Probabilities. On the basis of the decrease in the OH^\bullet radical concentrations, the reaction probabilities were determined for the different materials, as described in the Appendix, and the results are shown in Figure 2. The reaction probabilities differ by more than 2 orders of magnitude, with the reactivity being the least over TiO_2 and the greatest over Au. The reaction probability over gold is only a lower limit since the OH^\bullet radicals were almost completely consumed, even with the shallower bed.

The reproducibility in reaction probability is about $\pm 15\%$, but it is estimated that the error in the absolute value is $\pm 50\%$, except for the gold surface. Thus, for SiO_2 the reaction probability at 328 K was $(3.0 \pm 1.5) \times 10^{-3}$, which is in good agreement with the value of $(5.6 \pm 2) \times 10^{-3}$ reported by Gershenson et al.⁴ for quartz that had been treated with hydrofluoric acid. We found that treatment with hydrofluoric acid had almost no effect on the reaction probability for our SiO_2 sample. By contrast, dehydroxylation of the SiO_2 in He at 900°C caused a small, but significant, decrease in the reaction probability, as indicated by the curve labeled SiO_2 (heated). Iler¹² has pointed out that such a treatment results in extensive and largely irreversible dehydroxylation of the silica surface. Using infrared spectroscopy, we have confirmed that 90% of the water and hydroxyl groups were removed from the surface of the SiO_2 in the fused-quartz frit and that the surface species were not

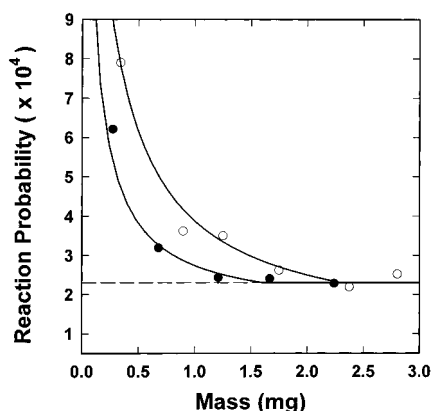


Figure 3. Variation in OH• reaction probability as a function of the amount of TiO₂ loaded onto a fused-quartz frit: (●) anatase, (○) rutile. The dashed line represents the reaction probability for both forms of TiO₂.

restored after 10 days in humid air at 300 K. Within the limits given for reproducibility, the reaction probabilities remain essentially constant for all of the examples shown in Figure 2 over the temperature range that is reported. There does, however, appear to be a consistent increase in reactivity over TiO₂ (anatase) that corresponds to an activation energy of about 4 kJ mol⁻¹.

Determination of the reaction probability for titania was somewhat more complicated because of the relatively large reaction probability over SiO₂ and the fact that the TiO₂ was supported on the fused-quartz frit. The variation in reaction probability as a function of the amount of TiO₂ is depicted in Figure 3, from which it is evident that on both the anatase and the rutile samples, the probability reaches a constant value of 2.3×10^{-4} at 308 K. Thus, the phase of TiO₂ does not affect the reaction probability. The solid lines in Figure 3 represent the expected reaction probabilities for the TiO₂/SiO₂ system assuming that the fraction of the surface covered by TiO₂ was proportional to the amount of TiO₂ and that coverage was complete at a loading of 1.6 mg for anatase and 2.0 mg for rutile. A scanning electron microscope (SEM) image of the frit with 1.8 mg of TiO₂ indicated that at this loading the titania essentially covered the silica surface.

Several additional experiments were carried out to determine the effect of other variables. With anatase on the frit, the inlet hydroxyl radical concentration was varied by a factor of 4 as a result of changing the microwave power, and it was observed that the reaction probability remained constant within the level of reproducibility. Similar results also were obtained over SiO₂. This observation supports the hypothesis that the reaction is first order with respect to hydroxyl radicals (Appendix).

Since H• atoms are undoubtedly produced in the microwave discharge along with OH• radicals, it was of interest to explore the possible effect of the H• atoms on the surface reaction probability. Molecular oxygen was added to the H₂O/He mixture with the expectation that the O₂ would remove H• as HO₂• according to the reaction



for which $k_1 = 4.7 \times 10^{12} \text{ mol cm}^{-3} \text{ s}^{-1}$ at 308 K.¹³ The reactions

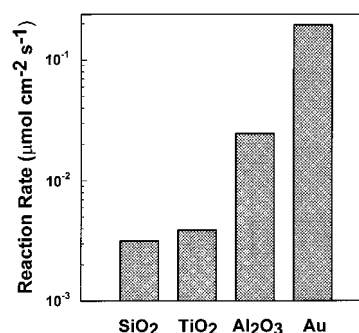
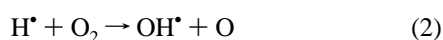
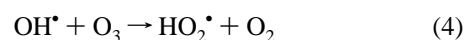
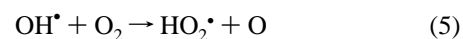


Figure 4. Hydrogen peroxide decomposition rate over SiO₂, TiO₂ (anatase), α-Al₂O₃ and Au obtained in a 30% aqueous solution of H₂O₂ at 323 K.

have rate constants that are more than 10 orders of magnitude less than the value for reaction 1. If H• atoms were providing a channel for the surface reaction of OH• radicals, one might expect that the presence of O₂ would decrease the measured reaction probability. In fact, at a H₂O partial pressure of 280 mTorr, the presence of 280 mTorr of O₂ caused the reaction probability at 308 K to increase from 2.1×10^{-3} to 5.2×10^{-3} over SiO₂ and from 2.0×10^{-4} to 3.5×10^{-4} over TiO₂. The origin of the positive effect of O₂ is unclear; however, the reaction



for which $k_4 = 4.5 \times 10^{10} \text{ mol cm}^{-3} \text{ s}^{-1}$, may play a role. Ozone would be formed in the microwave discharge. The reaction



is very slow at 308 K and would not contribute significantly to the loss of OH• radicals.

For certain purposes it may be more useful to know the absolute rate of reaction of OH• radicals on a particular surface. The uncertainty in this rate is larger than that of the reaction probability because the determination of the rate requires a value for the absolute OH• radical concentration and the residence time in the reactor zone. The former was determined using the procedure given in ref 3, and the latter was evaluated from the free volume and the gas flow rate (Appendix). At 308 K and a hydroxyl radical concentration of $4 \times 10^{12} \text{ molecules cm}^{-3}$, the rates of reaction are 1×10^{13} and $1 \times 10^{14} \text{ molecules cm}^{-2} \text{ s}^{-1}$ for TiO₂ and SiO₂, respectively. For TiO₂, complete surface coverage would occur in about 100 s. This means that for the experiments described here, which were carried out on a time scale of several hours, the OH• radicals were being consumed in a continuous cycle, in contrast to a stoichiometric reaction with certain sites on the surface.

Hydrogen Peroxide Decomposition. When one considers the reactions that might occur as OH• radicals react on a surface, their coupling to form H₂O₂ is an obvious possibility. For this reason, the rate of H₂O₂ decomposition was determined over SiO₂, α-Al₂O₃, TiO₂ (anatase), and Au, and the results are given in Figure 4. With the exception of TiO₂ (anatase), the reactivities for OH• radical removal and H₂O₂ decomposition occur in the same sequence, with the activities being in the order Au > α-Al₂O₃ > SiO₂. The decomposition of H₂O₂ over TiO₂ was also anomalous in that the rate oscillated as shown in Figure 5. The value reported was determined from the slope of the straight line indicated in the figure; therefore, it is an average rate. A much slower rate, which was comparable to the background decomposition rate, was observed initially. In view of the

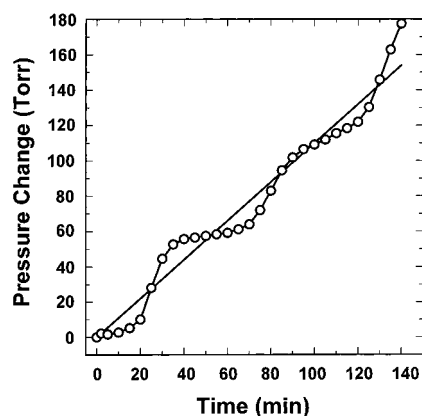


Figure 5. Oscillations during the decomposition of H_2O_2 over TiO_2 (anatase).

different rates for H_2O_2 decomposition over TiO_2 , it is uncertain where TiO_2 should be placed on the relative activity scale. The much slower rate would be more consistent with the order of reactivity for the OH^\bullet radical reaction.

Theoretical Analysis of OH^\bullet Chemisorbed on Gold Surfaces. A knowledge of the character of the chemical interaction between an OH^\bullet radical and a noble metal surface is necessary in order to understand features of the chemisorption and reactivity of OH on the gold surface. For this reason, we have determined cluster model wave functions which describe the electronic structure and the chemical interaction between OH and Au. A detailed analysis of the reaction kinetics would require an accurate knowledge of the potential surface over an extended region of values for the reaction coordinates. We have chosen instead to focus our theoretical work on the qualitative character of the OH–Au bonding. In particular, we present compelling evidence that the bonding of OH with these metal surfaces is dominantly ionic and that chemisorbed OH is essentially an $(\text{OH})^-$ anion. A special value of ab initio wave functions for cluster models of chemisorption is that they can be used to definitively characterize and distinguish ionic from covalent bonding of adsorbates on surfaces.¹⁴ This analysis of bond character cannot be made as easily when semiempirical methods are used, especially since the bond character is often assumed a priori.

Theoretical studies¹⁵ have shown that halogen atoms, F, Cl, and Br, adsorbed on Ag(111) surfaces form ionic bonds with the electron-accepting halogens, X, becoming X^- anions. While there is a small covalent character for the bonding of Cl and Br with Ag(111), the interaction of F/Ag(111) is essentially at the ideal ionic limit. It is easy to rationalize the formation of these ionic bonds by noting that the electron affinities, EA's, of the halogens are large, ~ 3.5 eV. The energetic cost of removing an electron from the metal, in order to place it on the adsorbate, is the work function which can be approximated as ~ 5 eV for most metals, including Au and Ag. This cost is not quite recovered by the halogen EA of ~ 3.5 eV; there is a 1.5 eV deficit. However, this simple energetic balance neglects the response or polarization of the metal surface to the presence of a charged adsorbate. It is common to describe this substrate response in terms of the formation of an image charge.¹⁶ However, the description of the metal response as a polarization of the substrate charge distribution stresses the chemical changes induced by an ionic adsorbate,¹⁷ and we shall use this preferred terminology. The energy associated with the substrate polarization in response to the presence of ionic chemisorbed species has been theoretically determined in several cases.^{18,19} This energy is rather large and contributes significantly to the stability

of the ionic bond; it is more than sufficient to make up the 1.5 eV energy deficit between the halogen EA and the metal work function, ϕ .

The cluster model has been extensively and successfully used to describe the electronic structure and chemical bonding of adsorbates on metal, semiconductor, and insulator surfaces.^{14,20,21} In this model, the cluster is formed by including atoms of the substrate near an adsorbate and normally one or, possibly, a few atomic or molecular adsorbates are also included. A representative cluster would contain 10–30 substrate atoms, although both larger and smaller clusters have been used. Quantum mechanical methods are used to determine wave functions for the cluster and the properties of the wave functions, including their energies, are used to describe surface processes. A special advantage of the cluster model is that it allows the detailed theoretical study of local aspects of the chemisorption bond.

For the calculations described in this paper, Hartree–Fock self-consistent field, SCF, wave functions were determined for the clusters, and electron correlation effects were not taken into account. Later, we provide information about the SCF cluster calculations. Here, we describe how the binding energy of the cluster and adsorbate may be determined accurately with SCF wave functions; following the notation for bond energies in molecules, we call this binding energy the dissociation energy, D_e . The goal is to determine a reliable value of D_e for a metal cluster of n atoms plus OH^\bullet , M_nOH . A value for D_e may be described as

$$D_e = -E(\text{M}_n\text{OH}) + E(\text{M}_n) + E(\text{OH}) \quad (6)$$

where $E(\text{M}_n\text{OH})$ is the total energy of the M_nOH cluster and $E(\text{M}_n)$ and $E(\text{OH})$ are the energies of the neutral separated systems of the metal cluster and the OH^\bullet radical, respectively. The energy $E(\text{M}_n\text{OH})$ is evaluated at or near the equilibrium geometry of the chemisorbed OH moiety. When a bond has a large degree of ionic character, Hartree–Fock, SCF values of D_e obtained using eq 6 are likely to have large errors because the SCF ionization potential, IP, and especially the SCF EA are not accurate.^{22,23} When the bond has substantial ionic character, it has been shown²⁴ that quite accurate values of D_e may be obtained by using experimental values for the EA and IP of the separated units and computing the SCF energies for dissociation to ionic limits. The appropriate formula for the case that OH is chemisorbed as OH^- is

$$D_e = -E(\text{M}_n\text{OH}) + E(\text{M}_n^+) + E(\text{OH}^-) + \text{EA}(\text{OH}) - \phi(\text{M}) \quad (7)$$

where $\phi(\text{M})$ is the work function of M, i.e., the energy required to remove an electron from the metal, and values for both EA and ϕ are taken from experiment.

The cluster used to study the interaction of OH^\bullet with the Au surface was chosen to describe the (100) surface of this fcc metal. It contains 14 metal atoms, 5 from the first, 4 from the second, and 5 from the third layer of the surface. This cluster is designed to simulate adsorption at an on-top site where the adsorbate is placed directly above the central atom of the first layer of the cluster. The geometric arrangement of the metal atoms, including the interatomic distances, is fixed at the bulk geometry and the clusters represent the unrelaxed and unreconstructed (100) surface of Au. The OH adsorbate is placed at the on-top site of the metal cluster with its internuclear axis perpendicular to the surface and with the O atom directed toward the surface. Following the usual convention, the z axis is taken

TABLE 1: Projections of the OH and OH[−] SCF Orbitals on the Cluster Wave Functions Which Model OH/Au^a

	OH orbitals	OH [−] orbitals
σ	5.95	5.95
π	3.91	3.95
total	9.86	9.90

^a The total projection is for the sum over all the occupied orbitals of OH; the σ and π contributions to the total are also given.

as the surface normal and the internuclear axis of chemisorbed OH is along z .

Hartree–Fock SCF wave functions for the clusters were computed using standard quantum chemical methods.^{25,26} In particular, the molecular orbitals were expanded in basis sets of contracted Gaussian-type orbital, CGTO, functions, and pseudopotentials described as effective core potentials, ECP's, were used to represent the core electrons of the metal atoms. The basis set ECP parameters are given by Hay and Wadt.²⁷ In order to avoid artifacts in the description of the chemical bonding that may arise from the use of ECP's, the valence and the outermost shells of core electrons were explicitly included for the adsorption site metal atom. The 19 electrons from the 5s²5p⁶5d¹⁰6s¹ shells were retained in the wave functions; these 19-electron ECP's incorporated relativistic mass–velocity and Darwin effects. For the “environmental” metal atoms which surround the adsorption site atom, fewer electrons need to be explicitly treated.²⁸ The Au environmental atoms were described by an 11-electron ECP where the electrons arising from the 5d¹⁰6s¹ shells were explicitly treated.

The CGTO basis sets for the adsorption site metal atoms were contracted to be of better than double- ζ , DZ, quality for the outer shells. In particular, three basis functions were used to describe the d shell and two basis functions each were used to describe the 6s and 6p “conduction band” shells. The same quality basis sets were used to describe the conduction band s and p shell of the environmental metal atoms; however, the 5d shell was described by a single CGTO. For the O and H atoms, better DZ quality basis sets were used; the CGTO basis set for O had 4s and 3p functions while that for H had 2s and 1p functions. For the basis set parameters for O and H see ref 29.

The wave functions for the Au₁₄OH cluster model of OH/Au(100) show that OH is reasonably strongly bound to the surface with an equilibrium bond distance of $z_e(\text{Au}–\text{O}) = 4.11$ bohr (~ 2.2 Å). In order to unambiguously determine the extent of the ionic character of the OH chemisorption bond to Au surfaces, we use a projection operator method²⁹ to obtain an effective charge for adsorbed OH. In this method, projection operators, $\hat{P}(\varphi_i) = \varphi_i \varphi_i^\dagger$ are formed using orbitals for the isolated OH molecule. The expectation value of the $\hat{P}(\varphi_i)$ over the cluster wave function, denoted $N_p(i)$, where $N_p(i) = \langle \Psi | \hat{P}(\varphi_i) | \Psi \rangle$, give measures of the occupations of the OH orbitals in the wave function for OH/Au. In particular, when $\langle \Psi | \hat{P}(\varphi_i) | \Psi \rangle \approx 2$, the space orbital φ_i is fully occupied in the cluster wave function and it does not participate in covalent chemical bonding with the substrate. The projection of the OH orbitals on $\Psi(\text{Au}_{14}\text{OH})$ given in Table 1 are for the metal–OH distance of $z = 4.1$ bohr, very near z_0 . Furthermore, the projections are made both with sets of OH SCF orbitals optimized for the neutral radical and for the closed shell anion, OH[−]. The nearly identical projections for the two sets of orbitals, (see Table 1) give strong support for projection of ~ 10 electrons associated with OH leading to an effective charge on OH of -1 . The projections in Table 1 are for the sum of the projections of the OH σ orbitals, $N_p(\sigma) + N_p(1\sigma) + N_p(2\sigma) + N_p(3\sigma)$, for the sum of the two degenerate spatial components of the 1 π

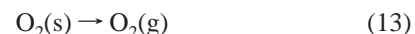
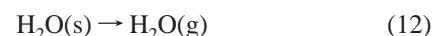
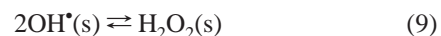
orbital, denoted $N_p(1\pi)$, and for the total projection, $N_p(\sigma) + N_p(1\pi)$. The value of the σ projection is almost 6. Since there are 6 σ electrons in either the isolated OH[•] radical or the OH[−] anion, the σ projection of 6 indicates that there is essentially no σ electron involvement in the bonding; in particular, there is no σ dative covalent bonding or donation from OH to the surface. The π projection is almost 4, indicating that the OH 1 π shell is essentially completely filled and that chemisorbed OH is an anion with 6 σ , 4 π , and a total of 10 electrons. The dipole moment curves for the frustrated translation of OH normal to the surface have a linear character^{14,30} that is fully consistent with the anionic character of OH. An important and key conclusion of the theoretical analysis of OH/Au is that the bonding is essentially ionic with OH being essentially an anion and with little, if any, covalent contribution to the bond. As discussed above, the ionic bonding of a good electron acceptor with a metal surface is expected to be reasonably strong.

The adsorption energy, D_e , of OH/Au was estimated using eq 7. The directly computed D_e for the cluster SCF wave functions was obtained for dissociation of Au₁₄OH to the ionic limits of Au₁₄⁺ and OH[−]. This directly computed value was then corrected for dissociation to neutral limits, as shown in eq 7, with experimental values for the work function, ϕ ,²⁹ and for the EA of OH[−].³⁰ The resulting energy was $D_e = 1.61$ eV (155 kJ mol^{−1}) for OH/Au (100).

The calculated D_e 's depend on the size of the metal clusters used,¹⁵ and it should be cautioned that the calculated values will change when larger clusters are used. Even if the changes with metal cluster size would reduce the D_e for the Au₁₄ cluster by as much as ~ 1 eV, the ionic bonding of OH to Au surfaces is still reasonably strong.

IV. Discussion

The observation that the reaction probability for OH[•] radicals and the catalytic decomposition of H₂O₂ display a similar reactivity pattern for SiO₂, α -Al₂O₃, and Au surfaces suggests that there may be a common mechanistic scheme for the two processes. The following mechanism is consistent with these results:

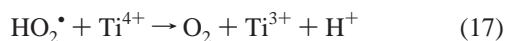
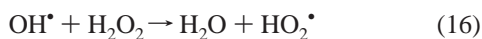


where reaction 10 is the rate-determining step. Here we use radical notation for all three surfaces even though OH[−], associated with a positive image charge, is present on the Au surface. The decomposition of H₂O₂ is initiated by the reverse of reaction 9, and the strength of the bond between OH[•] and the surface is important in establishing the surface concentration of this species. If reactions 8 and 9 approach equilibrium, the same concentration of OH[•](s) could be reached either by reacting OH[•] with the surface or by decomposing H₂O₂. The moderately large value of D_e that was determined for OH–Au is consistent with the relatively large activity of the gold surface for both reactions. In addition, the ionic character of OH may influence

its activity in reaction 10. The dissociation energy for OH• on the oxide surfaces is not known, but it is expected to be small on the covalent SiO₂ and the closed-shell oxide, Al₂O₃. On these two materials, it is unlikely that an anion would be formed from OH•, although hydroxide ions occur on Al₂O₃ as a result of the heterolytic dissociation of H₂O.

Because of reaction 10, the disappearance of OH• radicals and the decomposition of H₂O₂ would differ in absolute rates. Clearly, the concentrations of H₂O₂(s) and OH•(s) would not be the same if the experiment were carried out in a 30% aqueous solution of H₂O₂ or in a stream of OH• radicals that was produced in a microwave discharge.

In place of this mechanism, which is proposed for H₂O₂ decomposition over α-Al₂O₃, SiO₂, and Au, another pathway may occur over TiO₂. Among the four materials, titania is unique in that multiple oxidation states (Ti(III)) and Ti(IV)) are accessible. Moreover, H₂O₂ is both an oxidizing and a reducing agent.³³ Matthews³⁴ has proposed that for Ti³⁺,⁴⁺ a Fenton-type process may be involved. A mechanism that is analogous to the one proposed by Barb et al.³⁵ for the decomposition of H₂O₂ in a solution of Fe²⁺,³⁺ may be written as



Although reaction 16 in this mechanism and reaction 10 in the previous mechanism are the same, the overall rates of H₂O₂ decomposition could be very different because in the purely radical mechanism the formation of OH• is only via the reverse of reaction 9, whereas in the redox mechanism, OH• may be formed by reaction 15. This additional pathway may account for the larger average rate of H₂O₂ decomposition over TiO₂ relative to that over SiO₂ and Al₂O₃. An interpretation of the oscillating behavior with respect to the rate would be conjecture at this point; however, other similar examples of chemical oscillation in a redox system are known, such as the IO₃[−]/I₂ catalyzed decomposition of H₂O₂.³⁶ The smaller OH• radical reaction probability over the TiO₂ surfaces may be related to a smaller heat of adsorption or sticking coefficient for OH•. Thus, a significant fraction of the radicals that collide with the surface returns to the gas phase without further reaction. In fact, based on the analysis, only about 2 in 10⁴ of the radicals react during a collision. There was no evidence that photodesorption of OH• radicals occurred as a result of the interaction of laser photons with the H₂O/TiO₂ system.

A remaining issue that needs to be resolved is the origin of the very large differences in reaction probabilities between those that we and Gershenzon et al.⁴ observed and those that have been reported by Fisher and co-workers^{5,6} and Buss and co-workers¹¹ for the reaction of OH• radicals on SiO₂ at about 300 K. The respective values are about (2–5) × 10^{−3} and 0.4–0.6. The most obvious experimental variation is the origin of the SiO₂, with the much smaller reaction probabilities being observed over fused quartz. In one case, Fisher and co-workers^{5,6} measured their sticking coefficients *during* deposition of SiO₂ on a silicon substrate. The SiO₂ was derived from a tetraethoxysilane (TEOS)/O₂ plasma. In another study,¹¹ the value was determined for an oxidized silicon nitride film, using an H₂O plasma as the source of radicals. In both of these cases, the

nature of the SiO₂ surface may have been quite different from that of fused quartz, particularly with respect to defect structure. Fisher and co-workers⁶ suggested that the reaction probability may involve abstraction of a hydrogen atom from SiOH groups, but our results indicate that the extent of surface hydroxylation is only a secondary factor in OH• radical removal. Hydrocarbon and other impurities derived from TEOS could play a role in OH• radical reactions when this was used as the source of SiO₂, but with the pure H₂O plasma, such impurities would be minimal. On the basis of the published results and those reported here, it appears that the large differences in reaction probability are a result of variations in the surface of SiO₂.

V. Summary and Conclusions

The probability that a OH• radical will react when it collides with a surface depends strongly on the chemical composition of the solid phase. Among the several materials that were studied, the magnitude of the reaction probability was found to be in the order Au > α-Al₂O₃ > SiO₂ > TiO₂(anatase) = TiO₂(rutile). Since the experiments were carried out under steady state conditions, the OH• radicals were continuously reacting on the surface, presumably to form H₂O₂ as the initial product. To complete the catalytic cycle, H₂O₂ is decomposed to form H₂O and O₂. For Au, α-Al₂O₃, and SiO₂, the relative rates of aqueous H₂O₂ decomposition are in the same order as the OH• radical reaction probability, which suggests a common mechanism for the two processes. According to a radical mechanism that is proposed, the rate of reaction will be proportional to the concentration of OH on the surface. A theoretical analysis has shown that the chemisorption bond of OH on Au is dominantly ionic with adsorbed OH becoming the anion, OH[−]. For a good electron acceptor, like OH, ionic bonding leads to a reasonably strong chemisorption bond which may be as large as 155 kJ mol^{−1}. Furthermore, ionic chemisorption bonds do not have a strong directional character³⁵ and, thus, barriers to diffusion of OH[−] along the surface are expected to be small. All of these features are consistent with the large activity of Au. It is expected that the adsorption energy and the OH concentration on the close shell oxides, α-Al₂O₃ and SiO₂, would be smaller than on Au. Titania is anomalous in that the average rate of H₂O₂ decomposition is greater than would be expected on the basis of the OH• radical reaction probability. A redox mechanism is proposed for H₂O₂ decomposition, which could be responsible for the larger rate of reaction when H₂O₂ is derived from an aqueous solution. The OH• radical reaction probability of only 10^{−4} probably results from a small adsorption energy or sticking probability. Thus, in photocatalytic applications for the destruction of organic materials, OH• radicals that are formed on TiO₂ would remain available as reactive intermediates.

Acknowledgment. This research was supported by the Office of Basic Energy Sciences, U.S. Department of Energy.

Appendix: Determination of the Reaction Probability

The reaction probability is defined as the ratio of the number of OH• radicals on a surface to the total number of collisions. If one assumes that the reaction is first order with respect to the number of OH• radicals (see above), it follows that

$$\ln \frac{[\text{OH}]_0}{[\text{OH}]_t} = \ln R = kt \quad (\text{A1})$$

where [OH]₀ and [OH]_t are the radical concentrations before and after reaction with the catalyst, *k* is the rate constant, and

t is the residence time of the radicals within the frit or the shallow bed composed of the cylinders. The rate of reaction for the radicals, which may be expressed as molecules per second, is

$$\gamma_r = k[\text{OH}]V_f \quad (\text{A2})$$

where V_f is the free volume within the reaction zone (i.e., the difference between the total volume and the volume occupied by the solid phase). By combining eqs 1 and 2, γ_r can be expressed as

$$\gamma_r = (\ln R)F[\text{OH}] \quad (\text{A3})$$

Here, F is the gas flow rate, which is related to the residence time by $t = V_f/F$. The total collision rate of OH^\bullet radicals with the surfaces is given by

$$\gamma_{\text{tot}} = \frac{1}{4}\bar{c}A[\text{OH}] \quad (\text{A4})$$

where \bar{c} denotes the mean speed of the OH^\bullet radicals and A is the surface area of the material. The reaction probability, S , is then

$$S = \frac{\gamma_r}{\gamma_{\text{tot}}} = \frac{4F \ln R}{\bar{c}A} \quad (\text{A5})$$

References and Notes

- (1) Frost, A. A.; Pearson, R. G. *Kinetics and Mechanism*; Wiley: New York, 1953; p 114.
- (2) Lunsford, J. H. *Angew. Chem., Int. Ed. Engl.* **1995**, *34*, 970.
- (3) Hewett, K. B.; Anderson, L. C.; Rosynek, M. P.; Lunsford, J. H. *J. Am. Chem. Soc.* **1996**, *118*, 6992.
- (4) Gershenzon, Yu. M.; Ivanov, A. V.; Kucheryavyi, S. I.; Rozenshtein, V. B. *Kinet. Katal.* **1986**, *27*, 1069.
- (5) Bogart, K. H. A.; Cushing, J. P.; Fisher, E. R. *Chem. Phys. Lett.* **1997**, *267*, 377.
- (6) Bogart, K. H. A.; Cushing, J. P.; Fisher, E. R. *J. Phys. Chem. B* **1997**, *101*, 10016.
- (7) Noda, H.; Oikawa, K.; Ohya-Nishiguchi, H.; Kamada, H. *Bull. Chem. Soc. Jpn.* **1994**, *67*, 2031 and references therein.
- (8) Tevault, D. E.; Talley, L. D.; Lin, M. C. *J. Chem. Phys.* **1980**, *72*, 3314.
- (9) Noda, S.; Nishioka, M.; Harano, A.; Sadakata, M. *J. Phys. Chem. B* **1998**, *102*, 3185.
- (10) Morrow, B. A.; Ramamurthy, P. *J. Phys. Chem.* **1973**, *77*, 3052.
- (11) Fisher, E. R.; Ho, P.; Breiland, W. C.; Buss, R. J. *J. Phys. Chem.* **1993**, *97*, 10287.
- (12) Iler, R. H. *The Chemistry of Silica*; Wiley: New York, 1979; p 645.
- (13) Westley, F.; Herron, J. T.; Cvetanovic, R. J.; Hampson, R. F.; Mallard, G. NIST Chemical Kinetics Database, Version 3.0; National Institute of Standards and Technology, U.S. Department of Commerce, Washington, DC, 1991.
- (14) Bagus, P. S.; Illas, F. In *Encyclopedia of Computational Chemistry*; Schleyer, P. V. R., Allinger, N. L.; Clark, T.; Gasteiger, J.; Kollman, P. A.; Schaefer, H. F.; Eds.; Wiley: Chichester, UK, 1998; Vol. 4, p 2870.
- (15) Bagus, P. S.; Pacchioni, G.; Philpott, M. R. *J. Chem. Phys.* **1989**, *90*, 4287.
- (16) Lang, N. D.; Kohn, W. *Phys. Rev. B* **1973**, *7*, 354.
- (17) Garcia-Hernandez, M.; Bagus, P. S.; Illas, F. *Surf. Sci.* **1998**, *409*, 69.
- (18) Petereresson, L. G. M.; Bagus, P. S. *Phys. Rev. Lett.* **1986**, *56*, 500.
- (19) Pacchioni, G.; Bagus, P. S. *Surf. Sci.* **1992**, *269*, 269/270.
- (20) Bagus, P. S.; Pacchioni, G.; Nelin, C. J. In *Studies in Physical and Theoretical Chemistry*; Carbo, R., Ed.; Elsevier: Amsterdam, 1989; Vol 62, p 475.
- (21) Pacchioni, G. *Heterogeneous Chem. Rev.* **1996**, *2*, 213.
- (22) Bagus, P. S. In *Plasma Synthesis and Etching of Electronic Materials*; Chang, R. T. H., Abeles, B., Eds.; Materials Research Society Symposia Proceedings; Materials Research Society: Pittsburgh, PA, 1985; Vol. 38, p 179.
- (23) Bagus, P. S.; Illas, F. *Phys. Rev. B* **1990**, *42*, 10852.
- (24) Bagus, P. S.; Nelin, C. J.; Bauschlicher, C. W. Jr. *J. Chem. Phys.* **1983**, *79*, 2975.
- (25) Schaefer, H. F. *The Electronic Structure of Atoms and Molecules*; Addison-Wesley: Reading, MA, 1979.
- (26) Szabo, A.; Ostlund, N. S. *Modern Quantum Chemistry*; MacMillan: New York, 1982.
- (27) Hay, P. J.; Wadt, W. R. *J. Chem. Phys.* **1985**, *82*, 270.
- (28) Bagus, P. S.; Bauschlicher, C. W. Jr.; Nelin, C. J.; Laskowski, B. C.; Seel, M. *J. Chem. Phys.* **1984**, *81*, 3594.
- (29) van Duijneveldt, F. B. *IBM Res. Rep.* **1971**, No. RJ945.
- (30) Nelin, C. J.; Bagus, P. S.; Philpott, M. R. *J. Chem. Phys.* **1987**, *87*, 2170.
- (31) *CRC Handbook of Chemistry and Physics*, 76th ed.; CRC Press: Boca Raton, FL, 1995.
- (32) Huber, K. P.; Herzberg, G. *Molecular Spectra and Molecular Structure: IV. Constants of Diatomic Molecules*; Van Nostrand Reinhold: New York, **1979**.
- (33) Greenwood, N. N.; Earnshaw, A. *Chemistry of the Elements*; Pergamon: New York, 1984; p 746.
- (34) Matthews, R. W. *J. Chem. Soc., Faraday Trans. 1* **1984**, *80*, 457.
- (35) Barb, W. G.; Baxendale, J. H.; George, P.; Hargrave, K. R. *Trans. Faraday Soc.* **1951**, *47*, 591.
- (36) Bray, W. C. *J. Am. Chem. Soc.* **1921**, *43*, 1262.
- (37) Pacchioni, G.; Illas, F.; Philpott, M. R.; Bagus, P. S. *J. Chem. Phys.* **1991**, *95*, 4678.